Supplement of Atmos. Chem. Phys., 25, 8493–8505, 2025
https://doi.org/10.5194/acp-25-8493-2025-supplement

Atmospheric Chemistry and Physics
Open Access
EGU

Supplement of

Technical note: Towards a stronger observational support for haze pollution control by interpreting carbonaceous aerosol results derived from different measurement approaches

Yuan Cheng et al.

Correspondence to: Jiu-meng Liu (jiumengliu@hit.edu.cn)

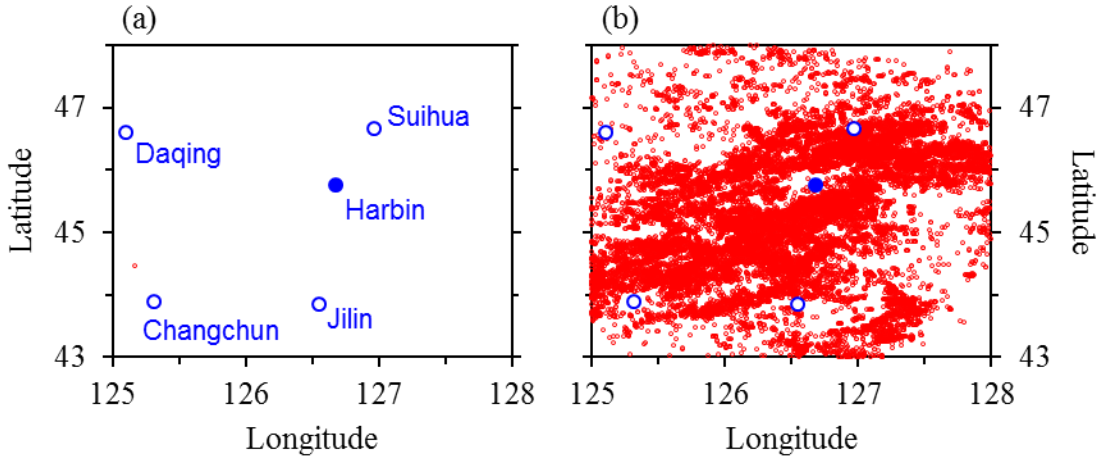

Figure S1. Fire hotspots (red circles) detected during the **(a)** winter and **(b)** spring campaigns by the joint NASA–NOAA Suomi National Polarorbiting Partnership (S-NPP) satellite. The locations of Harbin and several nearby cities are shown by the blue circles.

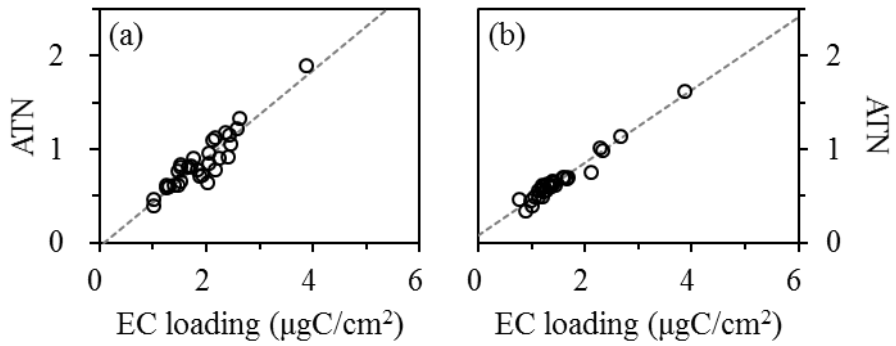

Figure S2. Relationships between ATN and EC loading, i.e., EC_s, for the **(a)** untreated and **(b)** extracted LV filters collected in winter. The temperature protocol used was IMPROVE-A. Linear dependence was identified for the whole EC_s range, regardless of the pretreatment approach (i.e., with or without methanol extraction). As indicated by the dashed lines in (a) and (b), the regression slopes were 47.1 ±3.6 (with a close-to-zero intercept; r = 0.93) and 39.0 ±1.4 (with a close-to-zero intercept; r = 0.98) m^2/gC for the untreated and extracted filters, respectively.

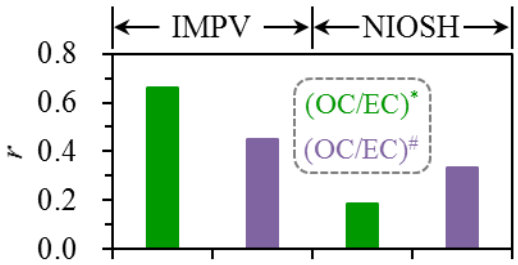

Figure S3. Comparison of *r* values derived from the linear regressions of various OC/EC estimations on SNA/CO, based on the wintertime LV samples. IMPV indicates the IMPROVE-A temperature protocol. A total of four sets of OC/EC ratios were determined using different protocols and pre-treatment approaches. The OC/EC ratio measured by the untreated samples using IMPROVE-A, i.e., the IMPV-based $(OC/EC)^{*}$, exhibited the strongest association with SNA/CO.

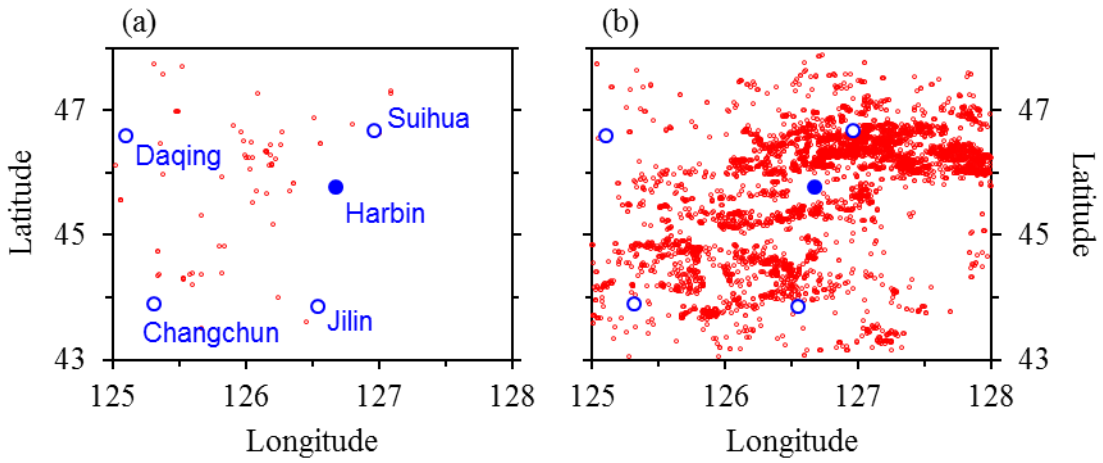

Figure S4. Fire hotspots (red circles) detected during two representative segments of the 2021 spring campaign, i.e., **(a)** 09:00 on April 27 to 16:00 on April 28, and **(b)** 21:00 on April 20 to 09:00 on April 22. Each period corresponded to three HV samples. The locations of Harbin and several nearby cities are shown by the blue circles. The period of (a) was characterized by sparse fire hotspots around Harbin, together with relatively low levels of LG/K^+ (below 1) and f_{LG} (below 1.5%). For the period of (b), the fire hotspots were much more intensive, accompanied with substantially increases in both LG/K^+ (reaching 1.7–3.3) and f_{LG} (reaching 5.3–6.5%). The contrast between fire hotspots detected during the periods of (a) and (b) provided clear evidence for the associations between agricultural fires and the two ratios. In addition, comparison of the spring and winter results suggested that a LG/K^+ ratio of ~0.5 was characteristic of household burning of biofuels, whereas the ratio could be effectively enhanced by agricultural fires. Here we used a threshold LG/K^+ of 1 to distinguish the events with considerable and insignificant impacts of agricultural fires. We also found that a common feature for the events with LG/K^+ above 1 was that the f_{LG} levels stayed above 1.8%, indicating a threshold LG/K^+ of 1 could be translated into a threshold f_{LG} of 1.8%. Finally, f_{LG} levels above 1.8% were used to identify the fire-impacted samples.

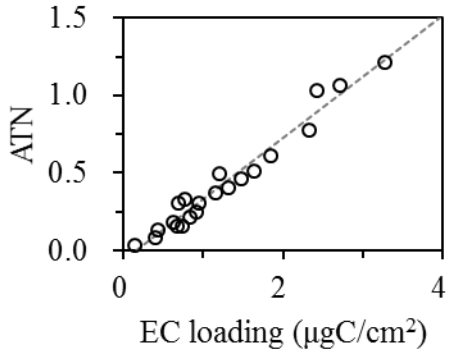

Figure S5. Relationship between ATN and EC loading, i.e., EC_s, for the untreated LV filters collected in spring. The temperature protocol used was IMPROVE-A. As indicated by the dashed line, a linear dependence was identified for the whole EC_s range. The regression slope was 39.6 ± 1.8 m^2/gC, with a close-to-zero intercept (r = 0.98).

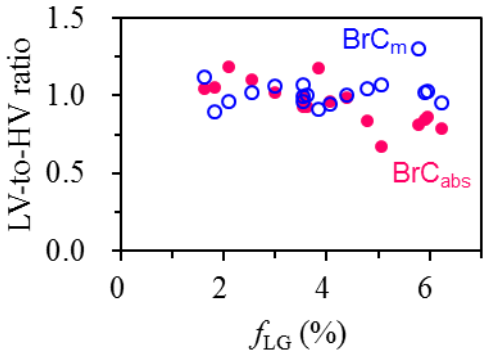

Figure S6. Dependences of the LV-to-HV ratios of BrC mass (BrC_m) and absorption (BrC_{abs}) on f_{LG} in spring.